Further Results on Hysteresis Compensation of Smart Micro-Positioning Systems with the Inverse Prandtl-Ishlinskii Compensator

Mohammad AL JANAIDEH, Micky RAKOTONDRABE, *IEEE, member* and Omar ALJANAIDEH

***Abstract*—A formula that characterizes the output of the inverse compensation is derived when the inverse Prandtl-Ishlinskii hysteresis model is applied as a feedforward compensator. For that the composition property as well as the initial loading curve of the Prandtl-Ishlinskii model are used to obtain this formula. We demonstrate therefore that the output of the feedforward controlled system is linear versus the input reference with an additional nonlinear and bounded term. To illustrate the interest of this theoretical result, we propose an experimental application with a piezoelectric actuator. First, we apply the Prandtl-Ishlinskii feedforward technique to control the piezoelectric actuator. Then, the formula of the previous theoretical result is used to construct an H_∞ feedback control from the feedforward controlled actuator. The experimental results demonstrate the efficiency of the calculated controller and therefore the benefits of the formula concerning the output of the inverse compensation.**

***Index Terms*—Prandtl-Ishlinskii model, feedforward control, inverse model, feedforward-feedback control, H_∞ synthesis, piezoelectric actuator.**

I. INTRODUCTION

SMart material-based actuators are becoming increasingly more popular for different micro- and nano-positioning applications such as observing and manipulating objects at micro and nano scale levels, see for example [1]–[3], and design high precision positioning systems, see for example [4]–[7]. However, these actuators exhibit hysteresis nonlinearities associated with oscillations in the open-loop systems responses, poor tracking performance and potential instabilities in the closed-loop system [8]–[10]. Different hysteresis models have been proposed to characterize the hysteresis nonlinearities in smart micro-positioning actuators. These models include the Preisach model [8], [11], the Prandtl-Ishlinskii model [1], [12]–[16], the Maxwell-Slip model [17], [18], the Bouc-Wen model [19], [20], and the Duhem model [21].

In order to enhance the tracking performance of hysteretic systems, considerable efforts have been made towards the design of control methods for compensating the hysteresis effects. These strategies can be classified into inverse-based hysteresis compensation methods and model-based hysteresis compensation methods. The inverse-based hysteresis compensation methods generally employ a cascade of a hysteresis model and its inverse together with a controller. These methods however necessitate an inverse formulation for the hysteresis model, which is often a challenging task [8]. On the other hand, the model-based hysteresis compensation methods employ the hysteresis model to design nonlinear controllers in order to compensate for the actuator hysteresis. These methods incorporate hybrid control [22], adaptive control [23], and energy-based [24] control, robust control [25], [26] or simple structured control such as PID [27]–[29].

The Prandtl-Ishlinskii model has been widely used for modeling and compensation of hysteresis nonlinearities in smart micro-positioning actuators, see for example [1], [9], [12], [16], [35]. Different studies show that the parameters of the Prandtl-Ishlinskii model can be easily identified and the model can be implemented with few play operators. Furthermore, the inverse Prandtl-Ishlinskii model that is used as a feedforward compensator is exact and can be obtained analytically. This makes the Prandtl-Ishlinskii model convenient for different real-time micro-and nano-positioning applications [1]. Owing to the characterization errors between the output of the Prandtl-Ishlinskii model and the measured output displacement of the smart micro-positioning actuator, the formulated inverse model is not exact and yields compensation errors in real-time applications.

However, it is shown that one of the main sources of the compensation errors when the inverse Prandtl-Ishlinskii model is used as a feedforward compensator is the inexactitude of the hysteresis model [30].

In a number of micro-and nano-positioning applications, the smart material-based actuators are coupled with a plant (dynamic system). In order to reduce the tracking errors between the reference input and the output of the plant, different studies proposed closed-loop control systems that consist of an inverse hysteresis model and a linear control method, see for example [3], [10], [31], [32]. The output of the inverse compensation, which is the output of the smart micro-positioning actuator in the presence of the inverse hysteresis model, is considered as an input signal to the plant. This signal can not be measured in a number of applications. Consequently, it is important to derive a mathematical formula that characterizes the output of the inverse compensation.

M. Al Janaideh is with the Department of Mechatronics Engineering, The University of Jordan, Amman 11942, Jordan, email: aljanaideh@gmail.com

M. RAKOTONDRABE is with the Department of Automatic Control and Micro-Mechatronic Systems, FEMTO-ST Institute, CNRS - University of Franche-Comté at Besançon (UFC) - ENSMM - UTBM, Besançon France, email: mrakoton@femto-st.fr

O. Aljanaideh is with the Department of Mechanical Engineering, The University of Jordan, Amman 11942, Jordan, and the Department of Automatic Control and Micro-Mechatronic Systems, FEMTO-ST Institute, CNRS - University of Franche-Comté at Besançon (UFC) - ENSMM - UTBM, Besançon France email: omaryanni@gmail.com

In this paper, a formula that characterizes the output of the inverse compensation when the inverse hysteresis model is used as a feedforward compensator is derived analytically. This formula facilitates employing model-based control methods along with inverse-based control methods in order to enhance the tracking performance of the smart micro-positioning actuators.

Consider Figure 1 where the input-output relationship of the smart micro-positioning actuator is a hysteresis modelled with the Prandtl-Ishlinskii technique and the inverse Prandtl-Ishlinskii model implemented in cascade is a hysteresis compensator (feedforward controller). It is important to note that the inverse Prandtl-Ishlinskii model is another Prandtl-Ishlinskii model. In general, the smart micropositioning actuator is presented by a Hammerstein system consisting of the Prandtl-Ishlinskii model cascaded with linear dynamics. In Figure 1, the output x is measured, while the measurements of the output y is not available.

The motivation of this paper is the need of analytical formula which describes the output of the inverse compensation when the inverse Prandtl-Ishlinskii model is used as a feedforward compensator. Due to the characterization errors of the model and uncertainties, the output of the inverse compensation yields compensation errors. Such formula can be used in closed-loop with feedback and feedforward control systems to enhance the performance of smart micro-positioning actuators in presence of model uncertainties.

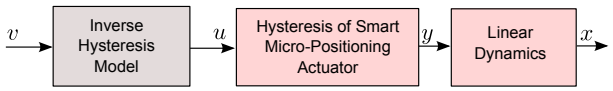

Fig. 1. Open-loop control system with hysteretic smart micro-positioning actuator presented by a Hammerstein system consists of the Prandtl-Ishlinskii model cascaded with linear dynamics. y is the output of the inverse compensation, u is the command input, and v is the reference input.

The contributions of the paper include the derivation of a formula that describes the output of the inverse compensation, $y\left(v(t),t\right)$, when the inverse Prandtl-Ishlinskii model, that is used as a feedforward compensator, is not exact. With this formula the error of the inverse compensation $\epsilon(t) = v(t) - y\left(v(t),t\right)$ can be obtained analytically. Experimental results demonstrate the efficiency of the approach by using the formula to construct an H_∞ linear feedback controller for a piezoelectric actuator.

The remainder of this paper is organized as follows. In Section II, we recall the Prandtl-Ishlinskii hysteresis model, the composition of two Prandtl-Ishlinskii models, the inverse Prandtl-Ishlinskii model, and the stop hysteresis operator. Section III states the main theoretical contribution of the study. In this section, the formula that characterizes the output of the inverse compensation is derived analytically. With this formula, the error of the inverse compensation is formulated. In Section IV, we represent the theoretical results of Section III with the threshold-discrete Prandtl-Ishlinskii model to calculate the thresholds and weights of the inverse threshold-discrete Prandtl-Ishlinskii model. In Section IV, we give an experimental case where the formula is used to synthesize an H_∞ controller that is used to control a piezoelectric actuator in closed-loop control system. Conclusions of the paper are presented in Section VI.

II. The Prandtl-Ishlinskii Model and its Inverse Considering the Initial Loading Curve

The Prandtl-Ishlinskii model and its inverse are presented in this section considering the initial loading curve and its inverse. This section is essential to derive a formula that can characterize the output of the inverse compensation.

A. The Prandtl-Ishlinskii model

The Prandtl-Ishlinskii model is based on the concept of a one-parameter family $(\mathcal{F}_r)_{r>0}$ of play operators parameterized by the threshold r. Recall that for an input function u which is monotone (non-decreasing or non-increasing) in each interval $[t_{i-1}, t_i]$ of a partition $0 = t_0 < \cdots < t_m = T$ and for a given threshold $r > 0$, the output of play operator $\mathcal{F}_r$ is defined by the formula

$$\mathcal{F}_r[u](t) = \max(u(t) - r, \min(u(t) + r, \mathcal{F}_r[u](t_{i-1}))) \quad (1)$$

with initial condition $\mathcal{F}_r[u](0) = \max(u(0) - r, \min(u(0) + r, 0))$. The definition can be extended to the whole space $C[0,T]$ of continuous functions on $[0,T]$ by a density argument as in [33]. For a given input $u(t) \in C[0,T]$, the output of the Prandtl-Ishlinskii model can be expressed as

$$\mathcal{P}[u](t) = p_0 u(t) + \int_0^\infty p(r)\mathcal{F}_r[u](t)dr, \quad (2)$$

where p_0 is a positive constant and $p(r)$ is an integrable density function that vanishes for large values of r. It is reasonable to assume that there exists a constant R such that $p(r) = 0$ for $r > R$. The density function $p(r)$ is usually defined based on the experimental data [30].

The Prandtl-Ishlinskii model can be re-expressed as

$$\mathcal{P}[u](t) = \phi'(0)u(t) + \int_0^R \phi''(r)\mathcal{F}_r[u](t)dr, \quad (3)$$

where $\phi(r)$ is the initial loading curve which is described as the stress-strain curve under increasing load, from $r = 0$ to $r = R$. The initial loading curve is defined for the thresholds $r > 0$ as [33]

$$\phi(r) = p_0 r + \int_0^r p(\tau)(r - \tau)d\tau. \quad (4)$$

Then $p(r) = \phi''(r)$ and $p_0 = \phi'(0)$. We denote the Prandtl-Ishlinskii model $\mathcal{P}$ constructed with the initial loading curve ϕ as $\mathcal{P}_\phi$ and the output of the model as $y(t) = \mathcal{P}_\phi[u](t)$.

B. Composition Property of the Prandtl-Ishlinskii model

In this section we present the composition property of the Prandtl-Ishlinskii model. This property has been formulated by Pavel Krejčí in [34]. The composition property states that when the output u of the Prandtl-Ishlinskii model $\mathcal{P}_\sigma[v](t)$, such that $u = \mathcal{P}_\sigma[v](t)$, constructed with initial loading curve σ, is applied as an input to the Prandtl-Ishlinskii model $\mathcal{P}_\rho$

constructed with the initial loading curve ρ, the composition $\mathcal{P}_\rho \circ \mathcal{P}_\sigma$ can also be characterized by the Prandtl-Ishlinskii model $\mathcal{P}_\lambda$, where $\lambda(r) = \rho \circ \sigma(r)$. Analytically

$$\mathcal{P}_\lambda[v](t) = \mathcal{P}_\rho \circ \mathcal{P}_\sigma[v](t). \tag{5}$$

Then,

$$\mathcal{P}_\lambda[v](t) = \lambda'(0)v(t) + \int_0^R \lambda''(r)\mathcal{F}_r[v](t)dr\,, \tag{6}$$

where $\lambda''(r)$ is a density function and $\lambda'(0)$ is a positive constant.

C. The inverse Prandtl-Ishlinskii model

We use the initial loading curve concept and the composition property of the Prandtl-Ishlinskii model presented in the previous section to present the inverse Prandtl-Ishlinskii model $\mathcal{P}^{-1}$ with the initial loading curve. To obtain the exact inverse for the Prandtl-Ishlinskii model, the output of the inverse compensation (see Figure 2) should yield

$$\mathcal{P}_\phi \circ \mathcal{P}^{-1}[v](t) = v(t), \tag{7}$$

where

$$\mathcal{P}^{-1}[v](t) = \psi'(0)v(t) + \int_0^Z \psi''(z)\mathcal{F}_z[v](t)dz\,, \tag{8}$$

where z is the positive threshold and ψ is an initial loading curve. Let

$$\psi(z) = g_0 z + \int_0^z g(\tau)(z-\tau)d\tau \tag{9}$$

and $\mathcal{P}^{-1}[v](t) = \mathcal{P}_\psi[v](t)$. Since $\mathcal{P}_\phi \circ \mathcal{P}_\psi = \mathcal{P}_{\psi\circ\phi}$, we conclude $\mathcal{P}_{\psi\circ\phi}[v](t) = v(t)$. Then

$$\mathcal{P}_{\psi\circ\phi}[v](t) = \eta'(0)v(t) + \int_0^R \eta''(r)\mathcal{F}_r[v](t)dr\,, \tag{10}$$

where $\eta(r) = \psi \circ \phi(r)$. To obtain exact inversion, the initial loading curve η should satisfy

$$\eta''(r) = 0 \tag{11}$$
$$\eta'(0) = 1 \tag{12}$$
$$\eta(0) = 0. \tag{13}$$

We can conclude

$$\eta(r) = r \tag{14}$$
$$z = \phi(r) \tag{15}$$
$$\psi = \phi^{-1}. \tag{16}$$

The initial loading curve ϕ of the Prandtl-Ishlinskii model $\mathcal{P}_\phi$ is convex, while the initial loading ψ of the inverse hysteresis model $\mathcal{P}_\psi$ is concave. It is important to mention that the Prandtl-Ishlinskii model is rate-independent model. Then, the inverse Prandtl-Ishlinskii model is a rate-independent feedforward compensator.

D. The stop operator

The output $\mathcal{E}_r$ of a stop operator is defined as [33]

$$\mathcal{E}_r[u](t) = \min(r, \max(-r, u(t) - u(0) + \mathcal{E}_r[v](t_i))) \tag{17}$$

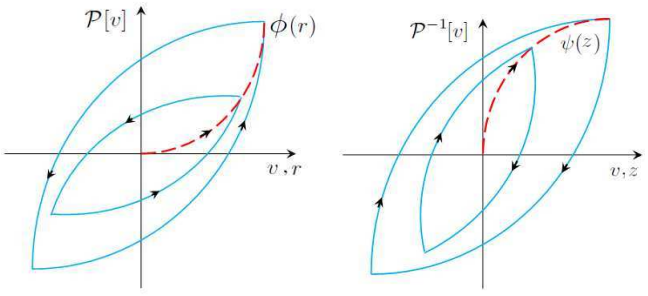

(a) (b)

Fig. 2. (a) Hysteresis loops of the Prandtl-Ishlinskii model $\mathcal{P}_\phi$ (solid) and initial loading curve ϕ (dashed line). (b) Hysteresis loops given by the inverse Prandtl-Ishlinskii model $\mathcal{P}^{-1}$ (solid line) and the initial loading curve ψ (dashed line).

where $\mathcal{E}_r[u](0) = \min(r, \max(-r, u(0)))$. From (17), it can be concluded

$$\mathcal{F}_r[u](t) + \mathcal{E}_r[u](t) = u(t). \tag{18}$$

The output of the stop operator is bounded by the threshold r. Analytically

$$-r \leq \mathcal{E}_r[u](t) \leq r. \tag{19}$$

The stop operator is used in Section III-B to study the boundedness of the error of the inverse compensation when the inverse Prandtl-Ishlinskii model is used as a feedforward compensator.

III. A Formula for the Output of the Inverse Compensation

Owing to characterization errors between the Prandtl-Ishlinskii model and the measured hysteresis loops, the formulated inverse Prandtl-Ishlinskii model yields compensation errors when used in the experiment as a feedforward compensator. Consequently, we assume that the identified model is an estimated model $\hat{\mathcal{P}}$. Then, the formulated inverse is an estimated inverse hysteresis model $\hat{\mathcal{P}}^{-1}$. In this section, we analytically derive the output of the inverse compensation $\mathcal{P} \circ \hat{\mathcal{P}}^{-1}$ when the inverse estimated Prandtl-Ishlinskii model $\hat{\mathcal{P}}^{-1}$ is applied as feedforward controller to the real hysteresis $\mathcal{P}$ which was approximated by the model $\hat{\mathcal{P}}$.

A. Analytical expression for $\mathcal{P} \circ \hat{\mathcal{P}}^{-1}$

The output of the inverse compensation $\mathcal{P} \circ \hat{\mathcal{P}}^{-1}$ can be expressed as

$$\mathcal{P}_\phi \circ \mathcal{P}_\psi[v](t) = \mathcal{P}_{\phi\circ\psi}[v](t). \tag{20}$$

Let

$$\mathcal{P}_{\phi\circ\psi}[v](t) = \mathcal{P}_\eta[v](t), \tag{21}$$

then

$$\mathcal{P}_\phi \circ \mathcal{P}_\psi[v](t) = p_{0\eta}v(t) + \int_0^R p_\eta(r)\mathcal{F}_r[v](t)dr, \tag{22}$$

therefore

$$\mathcal{P}\circ\hat{\mathcal{P}}^{-1}[v](t)=p_{0\eta}v(t)+\int_0^R p_\eta(r)\mathcal{F}_r[v](t)dr, \tag{23}$$

where $p_\eta(r)=\eta''(r)$ and $p_{0\eta}=\eta'(0)$. It is noted that the input-output relationship between the input v and the output of the inverse compensation $\mathcal{P}\circ\hat{\mathcal{P}}^{-1}[v]$ of the Prandtl-Ishlinskii model yields clockwise and counter-clockwise hysteresis loops. The density function of the inverse compensation $\mathcal{P}\circ\hat{\mathcal{P}}^{-1}[v]$ is $p_\eta(r)$. For $p_\eta(r)<0$, the output $\mathcal{P}\circ\hat{\mathcal{P}}^{-1}[v]$ yields concave initial loading curve, and for $p_\eta(r)>0$, the output $\mathcal{P}\circ\hat{\mathcal{P}}^{-1}[v]$ yields convex initial loading curve. Concave initial loading curve yields clockwise hysteresis loops, while convex initial loading curve yields counter-clockwise hysteresis loops. Figure 3 shows the output of the inverse compensation for $\mathcal{P}\circ\hat{\mathcal{P}}^{-1}$ for convex and concave initial loading curves.

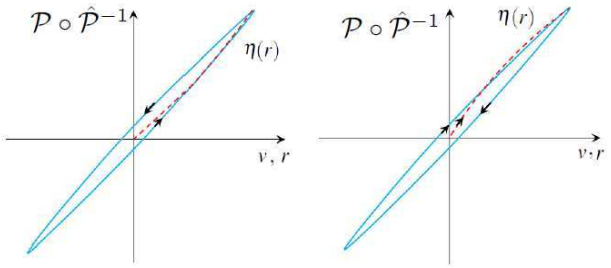

(a) (b)

Fig. 3. The output of the inverse compensation for $\mathcal{P}\circ\hat{\mathcal{P}}^{-1}$ with (a) convex $\eta(r)$, (b) concave $\eta(r)$.

B. Boundedness

A number of studies have assumed that the output of the inverse compensation can be decomposed into two terms. The first term describes a linear reversible term, while the second term is assumed to be bounded, see for example [31]. Analytically

$$\mathcal{N}\circ\hat{\mathcal{N}}^{-1}[v](t)=\rho v(t)+\Omega(t) \tag{24}$$

where $\mathcal{N}$ is a hysteresis model, $\hat{\mathcal{N}}^{-1}$ is the inverse of the estimated hysteresis model $\hat{\mathcal{N}}$, ρ is a positive constant, and $\Omega(t)$ is a nonlinear term bounded by a positive constant, $|\Omega(t)|\leq\xi$, where ξ is positive constant.

It is reasonable to assume that the parameters ρ and $\Omega(t)$ depend on the parameters of the model $\mathcal{N}$ and of its estimated inverse $\hat{\mathcal{N}}^{-1}$. In this section we use the analytical formulation for the output of the inverse compensation to show that the assumption (24) is true for the output of the inverse compensation $\mathcal{P}\circ\hat{\mathcal{P}}^{-1}$. Furthermore, we identify ρ and $\Omega(t)$ when $\mathcal{N}=\mathcal{P}_\phi$.

Using Equation (18), we conclude

$$\mathcal{P}_\phi\circ\mathcal{P}_\psi[v](t)=p_{0\eta}v(t)+\int_0^R p_\eta(r)\big(v(t)-\mathcal{E}_r[v](t)\big)dr, \tag{25}$$

then

$$\mathcal{P}_\phi\circ\mathcal{P}_\psi[v](t)=\rho v(t)-\int_0^R p_\eta(r)\mathcal{E}_r[v](t)dr, \tag{26}$$

where $\rho=p_{0\eta}+\int_0^R p_\eta(r)dr$. It follows from (26),

$$\mathcal{P}_\phi\circ\mathcal{P}_\psi[v](t)=\rho v(t)+\Xi(t), \tag{27}$$

where

$$\Xi(t)=-\int_0^R p_\eta(r)\mathcal{E}_r[v](t)dr. \tag{28}$$

Then,

$$\xi\leq|\int_0^R rp_\eta(r)dr|. \tag{29}$$

C. The error of the inverse compensation

The error of the inverse compensation with the inverse Prandtl-Ishlinskii model can be expressed as

$$\epsilon(t)=v(t)-\mathcal{P}\circ\hat{\mathcal{P}}^{-1}[v](t), \tag{30}$$

then

$$\epsilon(t)=v(t)\big(1-p_{0\eta}\big)-\int_0^R p_\eta(r)\mathcal{F}_r[v](t)dr \tag{31}$$

and

$$\epsilon(t)=v(t)\big(1-p_{0\eta}-\int_0^R p_\eta(r)\big)+\int_0^R p_\eta(r)\mathcal{E}_r[v](t)dr. \tag{32}$$

Then

$$\epsilon(t)=v(t)\big(1-\rho\big)+\int_0^R p_\eta(r)\mathcal{E}_r[v](t)dr \tag{33}$$

and

$$\epsilon(t)=v(t)\big(1-\rho\big)-\Xi[v](t). \tag{34}$$

Using Equations (27) and (28), we conclude that the error of the inverse compensation with the inverse Prandtl-Ishlinskii model can be expressed by a linear reversible term and a nonlinear bounded term.

IV. Threshold-Discrete Analysis

Remind that we denote with r the threshold parameter and p the weighting parameter of the Prandtl-Ishlinskii model. On the other hand, z is the threshold parameter and g the weighting parameter of the inverse model.

A. The threshold-discrete Prandtl-Ishlinskii model and its inverse

The output of the Prandtl-Ishlinskii model has to be expressed with the thresholds $0=r_0\leq r_1\cdots\leq r_N\leq r_{N+1}=R$ as

$$y=\mathcal{P}_\phi[u](t)=p_0u+\sum_{j=1}^{N}p(r_j)\mathcal{F}_{r_j}[u](t)\Delta r_j\,, \tag{35}$$

where N is the number of the play operators $\mathcal{F}_{r_j}$, $p(r_j)$ are positive weights. In discrete form, the initial loading curve (4)

can be expressed as

$$\phi(r_j) = p_0 r + \sum_{i=1}^{j} p(r_i)(r_j - r_i)\Delta r_i, \tag{36}$$

and

$$\phi'(r_j) = p_0 + \sum_{i=1}^{j} p(r_i)\Delta r_i. \tag{37}$$

In a similar manner, for $0 = z_0 \leq z_1 \cdots \leq z_N \leq z_{N+1} = Z$,

$$u = \mathcal{P}_\psi[v](t) = g_0 v + \sum_{i=1}^{N} g(z_i)\mathcal{F}_{z_i}[v](t)\Delta z_j, \tag{38}$$

where $\Delta z_j = z_{j+1} - z_j$ and

$$\psi(z_j) = g_0 z_j + \sum_{i=1}^{j} g(z_i)(z_j - z_i)\Delta z_i \tag{39}$$

and

$$\psi'(z_j) = g_0 + \sum_{i=1}^{j} g(z_i)\Delta z_i. \tag{40}$$

To obtain the parameters of the inverse, for $z \in [z_j, z_{j+1})$, where $j = 0, \cdots, N$, we use $\frac{d}{dr}(\psi \circ \phi(r)) = \frac{d}{dr} r$. Then $\phi'(r)\psi'(z) = 1$, where $z_j = \phi(r_j)$. We can write

$$z_j - z_{j-1} = (p_0 + \sum_{i=1}^{j-1} p(r_i)\Delta r_i)(r_j - r_{j-1}) \tag{41}$$

and

$$g_0 + \sum_{i=1}^{j} g(z_i)\Delta z_i = \frac{1}{p_0 + \sum_{i=1}^{j} p(r_i)\Delta r_i}. \tag{42}$$

We can write

$$g(z_j)\Delta z_j = -\frac{p(r_j)\Delta r_j}{(p_0 + \sum\limits_{i=1}^{j} p(r_i)\Delta r_i)(p_0 + \sum\limits_{i=1}^{j-1} p(r_i)\Delta r_i).} \tag{43}$$

Let $p_j = p(r_j)\Delta r_j$ and $g_j = g(r_j)\Delta r_j$, then we conclude

$$z_j - z_{j-1} = p_0 + \sum_{i=1}^{j-1} p_i(r_j - r_{j-1}) \tag{44}$$

and

$$g_j = -\frac{p_j}{(p_0 + \sum\limits_{i=1}^{j} p_i)(p_0 + \sum\limits_{i=1}^{j-1} p_i).} \tag{45}$$

B. Threshold-discrete inverse compensation output

This section presents the output and the error of the inverse compensation in discrete forms with a numerical example. In [37] and [38], the error of the inverse compensation for the discrete-threshold Prandtl-Ishlinskii model is presented with a linear term and a bounded nonlinear term for approximate hysteresis compensation.

The output of the inverse compensation can be written in the discrete form as

$$\mathcal{P} \circ \hat{\mathcal{P}}^{-1}[v](t) = p_{0\eta} v(t) + \sum_{j=1}^{N} p_{\eta j}\mathcal{F}_{r_j}[v](t)\Delta r_j. \tag{46}$$

That is, when using the stop operator,

$$\mathcal{P}_\phi \circ \mathcal{P}_\psi[v](t) = \rho v(t) - \sum_{j=1}^{N} p_{\eta j}\mathcal{E}_{r_j}[v](t)\Delta r_j. \tag{47}$$

The error of the inverse compensation can be expressed as

$$\epsilon(t) = v(t)\big(1-\rho\big) + \sum_{j=1}^{N} p_{\eta j}\mathcal{E}_{r_j}[v](t)\Delta r_j \tag{48}$$

Then

$$|\epsilon(t)| \leq |v(t)\big(1-\rho\big)| + |\sum_{j=1}^{N} p_{\eta j}\mathcal{E}_{r_j}[v](t)\Delta r_j| \tag{49}$$

and

$$|\epsilon(t)| \leq |v(t)\big(1-\rho\big)| + |\sum_{j=1}^{N} p_{\eta j} r_j \Delta r_j|. \tag{50}$$

Let $p^*_{\eta j} = p_{\eta j}\Delta r_j$ and $r_j = r_{\max}\varrho_j$, where $\varrho_j \leq 1$ are positive constants, then

$$|\epsilon(t)| \leq |v(t)\big(1-\rho\big)| + r_{\max}|\sum_{j=1}^{N} p^*_{\eta j}\varrho_j|. \tag{51}$$

and

$$|\epsilon(t)| \leq |v(t)\big(1-\rho\big)| + r_{\max}|\sum_{j=1}^{N} p^*_{\eta j}\varrho_j|, \tag{52}$$

where

$$p_{\eta\max} = \max\{|p^*_{\eta j}|\}. \tag{53}$$

Then we conclude

$$\sum_{j=1}^{N} p_{\eta j}\varrho_j \leq p_{\eta\,\max}\sum_{j=1}^{N}\frac{|p^*_{\eta j}|}{p_{\eta\,\max}}\varrho_j. \tag{54}$$

Since

$$\frac{|p^*_{\eta j}|}{p_{\eta\,\max}}\tau_j \leq 1 \tag{55}$$

we conclude

$$|\epsilon(t)| \leq |v(t)\big(1-\rho\big)| + N r_{\max} p_{\eta\max}. \tag{56}$$

It is important to mention that the boundedness of the nonlinear term in inverse compensation error was concluded in [36]–[38] for approximate hysteresis compensation.

C. Numerical example

In this section, we present a numerical example to show the capability of formula (46) to characterize the output of the compensation. We use $\mathcal{P}$ with the weights of $p_i = \{0.1, 0.0461, 0.069, 0.1029, 0.1535, 0.2291, 0.3417, 0.5098, 0.7605, 1.1345, 1.6925\}$ and the thresholds of $r_i = \{0, 4, 8, 12, 16, 20, 24, 28, 32, 36, 40\}$. The parameters of the inverse $\mathcal{P}^{-1}$ has been calculated and provide: $z_i = \{0, 0.4, 0.985, 1.85, 3.19, 5.00, 7.81, 11.98, 18.18, 27.44, 41.228\}$

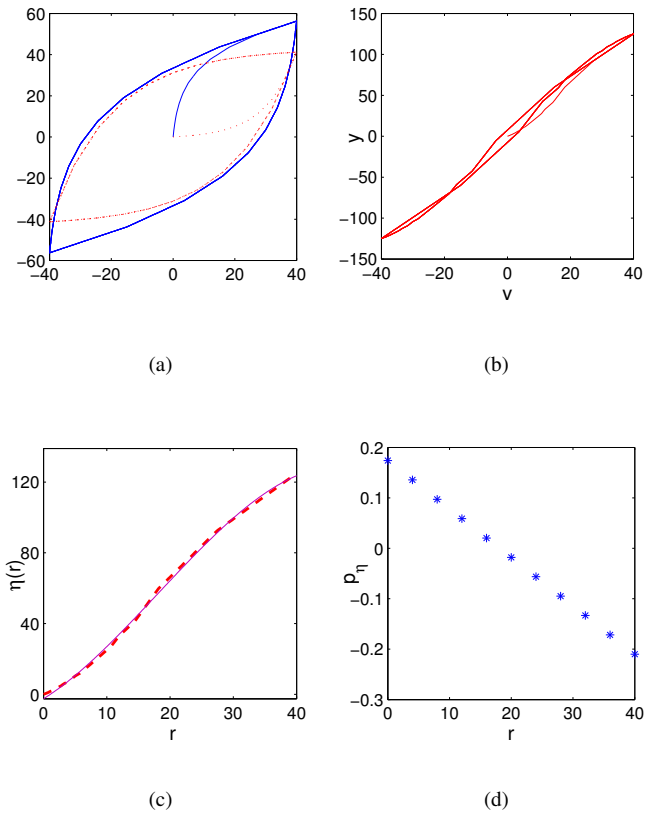

Fig. 4. Numerical example: (a) The output y of Prandtl-Ishlinskii model $\mathcal{P}[u]$ (dotted line) and the output u of the inverse estimated model $\hat{\mathcal{P}}^{-1}[v]$ (solid line), (b) The output of the inverse compensation $y = \mathcal{P} \circ \hat{\mathcal{P}}^{-1}[v]$ when the inverse estimated model $\hat{\mathcal{P}}^{-1}[v]$ is applied as feedforward compensator for the hysteresis nonlinearity of $\mathcal{P}[u]$, (c) comparison between the initial loading curve $\eta(r)$ obtained by (57) (solid line), and the initial loading curve of (58) (dashed line), and (d) the weights $p_{\eta i}$ of (58).

and $g_i = \{10, -3.16, -2.19, -1.5, -1.02, -0.69, -0.47, -0.31, -0.21, -0.143, -0.10\}$, which are the thresholds and the weights respectively. In order to estimate errors, instead of using the exact inverse $\mathcal{P}^{-1}$, we will use an estimated inverse Prandtl-Ishlinskii model $\hat{\mathcal{P}}^{-1} = 1.29\mathcal{P}^{-1}$ with $g_0 = 10.1$. The initial loading curve $\eta(r)$ of $\mathcal{P} \circ \hat{\mathcal{P}}^{-1}$ is characterized as

$$\eta(r) = -0.0016r^3 + 0.087r^2 + 2.2r + 2.5 \qquad (57)$$

and

$$y(t) = \mathcal{P} \circ \hat{\mathcal{P}}^{-1}[v](t) = 2.2v(t) + \sum_{i=1}^{10} p_{\eta i} \mathcal{F}_{r_i}[v](t). \qquad (58)$$

The weights of the nonlinear term include $p_{\eta i} > 0$ for $i = \{0, 1, 2, 3, 4\}$, $p_{\eta 5} = 0$, and $p_{\eta i} < 0$ for $i = \{6, 7, 8, 9, 10\}$. Figure 4 shows the simulation results. It can be noted that nonlinear concave-convex initial loading curve $\eta(r)$ yields counter-clockwise and clockwise hysteresis loops in the output of the inverse compensation $y(t)$. That is due to the positive and negative weights of the output of the inverse compensation.

V. Experimental Case: Applications to a Piezoelectric Actuator (PEA)

A. Presentation of the setup

Piezoelectric cantilevered actuators are widely used as precise manipulators in micromanipulation and microassembly of small objects [39], as actuators in miniaturized bio-inspired robots [40], as scanners in atomic force microscopy (AFM) [41], or also as actuators in micromirror orientation [42], [43]. Owing to the high-resolution positioning (in the order of nanometer-scale), the high-bandwidth output, and the high-stiffness, PEAs are very recognized in these various micro- and nano-positioning applications. However, these actuators show strong hysteresis nonlinearities. In this section, we used a piezoelectric actuator (PEA) with a cantilevered structure for the experiment.

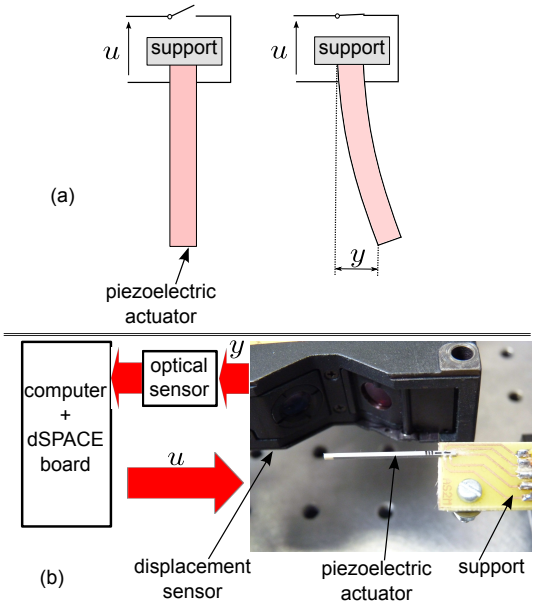

Fig. 5. (a) piezoelectric cantilevered actuator, and (b) the experimental setup.

The principle scheme of the PEA is depicted in Figure 5-a. This actuator is made of lead zirconate titanate (PZT) ceramics. The experimental setup is presented in Figure 5-b and is composed of:

- the piezoelectric cantilevered actuator (PEA) having total and active dimensions (active length × width × thickness) of: 15mm ×2mm ×2mm,
- an optical displacement sensor is used to measure the bending of the PEA. The sensor (LC2420 from Keyence) has a resolution of 10nm and a bandwidth up to 20kHz. However, a large bandwidth yields a noisy signal that is not convenient for this experiment and example. We have therefore tuned the sensor's bandwidth to be 4900Hz,
- a computer with Matlab-Simulink software which is used to manage the signals of the input voltage, the reference input, and the output displacement, and to implement feedback and feedforward controllers,

- and a dSPACE board which serves as DAC/ADC converter between the computer and the experimental setup. The sampling time of the computer and dSPACE board is set to 0.2ms which permits to account for the bandwidth of the PEA.

B. Characterization

To characterize the hysteresis nonlinearity of the PEA, a sinusoidal input voltage $u(t)$ is applied. The excitation frequency is chosen to be low enough ($f = 0.1$Hz) in order to avoid the phase lag in the measured output displacement. However, the excitation frequency should not be too low in order to avoid the creep effects in the output displacement [1]. Figure 6 pictures the input-output relationship between the input voltage $u(t)$ and the output displacement $y(t)$. Notice that ± 10V is the maximum range of the input voltage applicable to the PEA. As shown in Figure 6, the measured input-output relationship between the input voltage and the output displacement shows hysteresis percentage of 16.3% ($= \frac{h_{hyst}}{H_{hyst}} \approx \frac{14}{86}\mu$m/$\mu$m).

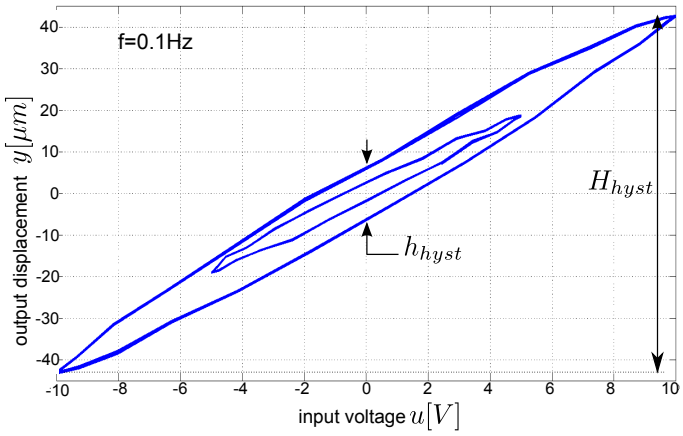

Fig. 6. Measured hysteresis loops of the PEA with $u(t) = 5\sin(2\pi 0.1t)\,V$ and $u(t) = 10\sin(2\pi 0.1t)\,V$.

C. Modeling and parameters identification

Figure 7 shows the Hammerstein model for the PEA with the Prandtl-Ishlinskii model $\hat{\mathcal{P}}[u]$ and the linear dynamics model $D(s)$. To identify the parameters of the Prandtl-Ishlinskii model $\hat{\mathcal{P}}[u]$, measured hysteresis loop with $u(t) = 10\sin(2\pi 0.1t)$V is used with its initial loading curve. We select 15 play operators and apply the identification procedure presented in [1]. The identified thresholds and weights are

$$\begin{cases} r_i = \{0.095, 0.38, 0.84, 1.46, 2.21, 3.07, 4.01 \\ \quad 4.98, 5.96, 6.89, 7.76, 8.52, 9.14, 9.61, 9.9\} \\ p_i = \{2.55, 0.57, 1.3, -1.57, 1.25, -0.054, -0.032, 0.66 \\ \quad 0.16, -0.77, 2.02, -1.63, -0.15, 2.99, -1.09\} \end{cases} \tag{59}$$

Figure 8 pictures the experimental hysteresis loops compared with the output of the Prandtl-Ishlinskii model $\hat{\mathcal{P}}$. This comparison shows that the model $\hat{\mathcal{P}}[u]$ acceptably fits with the measured hysteresis loop.

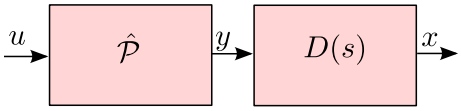

Fig. 7. Hammerstein model for the PEA, where $\hat{\mathcal{P}}$ is the Prandtl-Ishlinskii model and $D(s)$ is linear dynamics model.

To identify the linear dynamics model $D(s)$, a step input voltage of $u = 10$V is applied to the PEA. The step response displacement is recorded at the maximal sampling frequency of the acquisition board (sensors, dSPACE board) in order to have eventual higher resonant frequencies. The result is pictured in Figure 9, which shows an oscillation with a frequency of about 400Hz. Using the measured step response displacement and the ARMAX (Auto Regressive Moving Average with eXternal inputs) parametric identification technique [44], different model orders can be identified. The error between the measured step response and the output of each model $D(s)$ has been afterwards evaluated with the standard deviation as measure. It is shown that beyond eighth-order transfer function, the standard deviation of the error does not decrease substantially. We therefore use a transfer function $D(s)$ of order eight, see equation (60). Figure 9 pictures the comparison between the measured step response displacement and the output displacement of the linear model $D(s)$ of the scaled dynamics which shows a good agreement. From this model, the first two resonant frequencies can be determined as 596.8Hz and 9994.9Hz. Higher resonance frequencies certainly exist but they are outside the bandwidth of the measurement system, i.e. bandwidth of the sensor and of the used acquisition system.

$$D(s) = \frac{-20.7\big(s-1.22\times10^5\big)\big(s+2.99\times10^4\big)\big(s-2.776\times10^4\big)}{\big(s^2+925s+4.59\times10^5\big)\big(s^2+55s+1.4\times10^7\big)} \\ \frac{\big(s-1.07\times10^4\big)\big(s+1430\big)\big(s^2+4.3\times10^4 s+3.2\times10^9\big)}{\big(s^2+1.54\times10^4 s+4\times10^9\big)\big(s^2+964s+3.95\times10^9\big)} \tag{60}$$

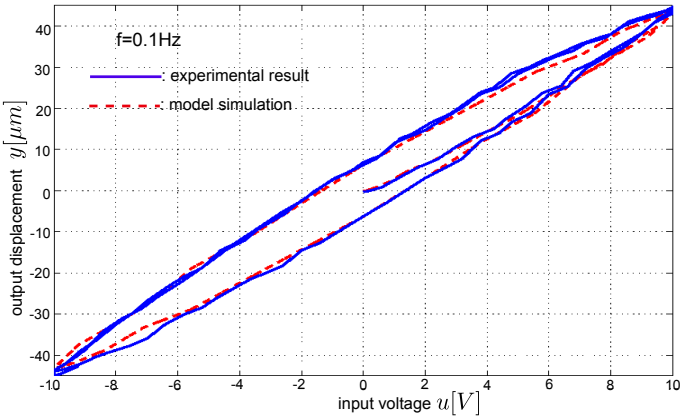

Fig. 8. Hysteresis of the PEA at 0.1Hz: comparison of the experimental result with the model simulation.

D. Hysteresis compensation using the inverse Prandtl-Ishlinskii model

The compensation for the hysteresis is then considered with the inverse Prandtl-Ishlinskii model as shown in Figure 10. In this figure, $\mathcal{P}$ represents the measured hysteresis loops of the PEA. The inverse model $\hat{\mathcal{P}}^{-1}$ is the compensator and is calculated as the inverse of the model $\hat{\mathcal{P}}[u]$ with parameters in equation (59). The inverse calculation is based on the method in [1] for example. We obtain the following thresholds and weights for the inverse model $\hat{\mathcal{P}}^{-1}$:

$$\begin{cases} z_i = \{0, 0.72, 2.16, 4.89, 7.04, 10.58, 14.36, 18.26, 22.81 \\ \quad 27.34, 30.85, 35.46, 38.24, 40.24, 42.35\} \\ g_i = \{0.39, -0.072, -0.094, 0.12, -0.11, 0.0033, 0.002 \\ \quad -0.035, -0.007, 0.04, -0.082, 0.06, 0.008, -0.095, 0.024\} \end{cases} \tag{61}$$

The inverse model $\hat{\mathcal{P}}^{-1}$ is then applied as a feedforward compensator to the PEA following the scheme in Figure 10. Figure 11 pictures the output of the inverse compensation $y = \mathcal{P} \circ \hat{\mathcal{P}}^{-1}[v]$ versus the input v. We can observe a slight hysteresis nonlinearity in the output of the inverse compensation that was not compensated by the inverse model $\hat{\mathcal{P}}^{-1}$. This hysteresis yields error in the output of the inverse compensation due to the fact that the identified model $\hat{\mathcal{P}}[u]$ is an approximation of the measured hysteresis loops $\mathcal{P}$. This error can be expressed as $\epsilon = v - \mathcal{P} \circ \hat{\mathcal{P}}^{-1}[v]$. This error has an amplitude of 3.75% ($= \frac{h_{hyst}}{H_{hyst}} \approx \frac{3}{80}\mu$m/$\mu$m). As demonstrated in Section. III-C, the error can be expressed by a linear reversible term and a nonlinear bounded term.

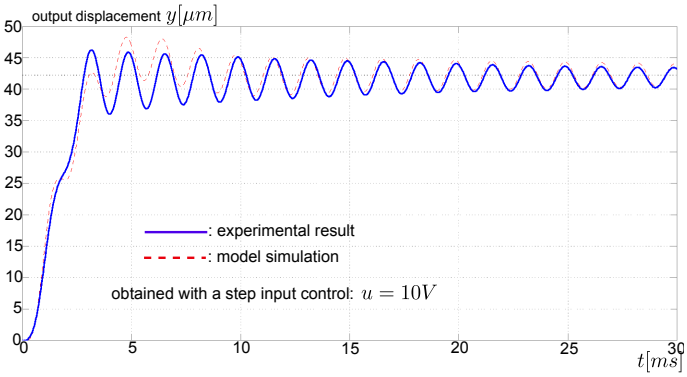

Fig. 9. Comparison between the step response displacement of the PEA and the output of $D(s)$ when $u = 10$V is applied.

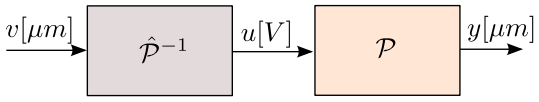

Fig. 10. Feedforward hysteresis compensation with the inverse Prandtl-Ishlinskii model.

E. H_∞ control of the piezoelectric actuator

In this subsection, we consider the feedback control of the output of the inverse compensation presented in Figure 11. In order to consider the dynamics of the PEA, the identified normalized dynamics $D(s)$ of (60) is also accounted for the feedback control. The system to be controlled has therefore the input $v[\mu$m] and the output $x[\mu$m] of the plant as depicted in Figure 12-a.

1) Model for the feedback control synthesis: As described in Section. III-C, the output of the inverse compensation $\mathcal{P}o\hat{\mathcal{P}}^{-1}[v]$ can be expressed by a linear operator ρ and a bounded nonlinear term Ω, that is

$$\begin{aligned} & y(t) = \mathcal{P}o\hat{\mathcal{P}}^{-1}[v(t)] = \rho v(t) + \Omega[v(t), t] \\ & \Leftrightarrow \\ & y(s) = \mathcal{P}o\hat{\mathcal{P}}^{-1}[v(s)] = \rho v(s) + \Omega[v(s), s]. \end{aligned} \tag{62}$$

With $D(s)$ (62), we have

$$\begin{aligned} & x(s) = D(s)y(s) = D(s)\mathcal{P}o\hat{\mathcal{P}}^{-1}[v(s)] \\ & = D(s)\left(\rho v(s) + \Omega[v(s), s]\right) \\ & \Leftrightarrow \\ & x = \rho D(s)v + \Omega_x \end{aligned} \tag{63}$$

where $\Omega_x = D(s)\Omega$ is an equivalent output disturbance and $G(s) = \rho D(s)$ is a linear dynamic system to be controlled. Figure 12-b pictures the new equivalent block diagram.

Our target is to obtain a linear controller $C(s)$ that permits the linear dynamic system $G(s)$ to conveniently track the desired input x_d and reject the disturbance Ω_x (see Figure 13-a) considering the tracking error $e = x_d - x$. An efficient way to consider the tracking specifications and the disturbance rejection during the controller synthesis is the H_∞ control technique.

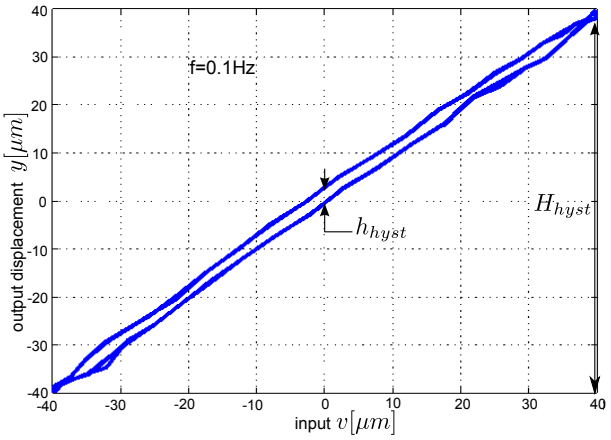

Fig. 11. The output of the inverse compensation.

The static gain ρ is identified considering the input-output relationship presented in Figure 10, from which we conclude $\rho = \frac{40\mu m}{40\mu m} = 1$. The nonlinear term Ω can also be characterized from Figure 10. An interesting characteristic of Ω is the case corresponding to the maximum hysteresis nonlinearity $\frac{h_{hyst}}{H_{hyst}}$. Then, we deduce that $y = 1v + \Omega$, where $|\Omega| \leq 3\mu m$. Since the linear dynamics $D(s)$ is normalized, the output disturbance $\Omega_x = D(s)\Omega$ has a bound of 3μm$\times(1 + \delta_D)$, where δ_D

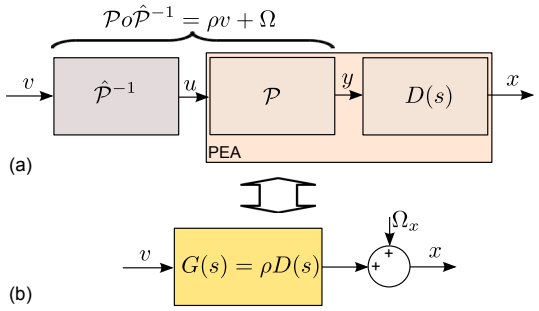

Fig. 12. The system to be controlled by a feedback controller.

is the overshoot and can be calculated from Figure 9 as $\delta_D = 9.5\%$. Consequently, the maximum error of Ω_x, that is denoted Ω_x^{max}, is $\Omega_x^{max} = 3.285\mu$m. This is used during the controller synthesis.

2) Specifications: The specifications used to calculate the H_∞ controller $C(s)$ are detailed below. These specifications are usually employed in micromanipulation and microassembly tasks with piezoelectric actuators similar to the PEA experimented in this study [39].

a) Tracking performance:

- the initial overshoot of 9.5% should be damped and should be equal to zero for the closed-loop system,
- the tracking error should be less or equal to 0.1%,
- and the settling time should be less or equal to 3ms.

b) Disturbance rejection: the effect of the disturbance Ω_x^{max} should be negligible at the output. Considering $\Omega_x^{max} = 3.285\mu$m, the maximum tracking error should be $e^{max} = 100$nm.

c) Command moderation: the used PEA is operated with an input voltage u between $+10$V and -10V which corresponds to an input v between $+42\mu$m and -42μm, respectively. In order to ensure that this maximal range of voltage will not be exceeded, we propose the following command moderation specification: a reference input x_d between $+40\mu$m and -40μm should yield a maximal driving input v of $+40\mu$m and -40μm. In such a way, we ensure that the operating driving voltage u is between $+10$V and -10V.

3) H_∞ problem: In order to account for the mentioned specifications, three weighting functions $W_1(s)$, $W_2(s)$ and $W_3(s)$ are introduced to the closed-loop scheme in Figure 13-a. We obtain the augmented closed-loop in Figure 13-b. These weighting functions are utilized for the tracking performance, command moderation, and disturbance rejection, respectively. Hence, the exogenous inputs for the synthesis are the reference x_d and the disturbance Ω_w, and the outputs to be controlled are the weighted outputs o_1 and o_2. From Figure 13-b, a standard scheme having the form of Figure 13-c can be constructed. The system P_{aug}, called as augmented system, includes the system $G(s)$ and the weightings $W_1(s)$, $W_2(s)$ and $W_3(s)$. The standard H_∞ problem consists therefore in finding an optimal value $\gamma > 0$ and a controller $C(s)$ stabilizing this standard scheme and guaranteeing the following inequality [45]:

$$\left\| F_l\left(P_{aug}, C\right) \right\|_\infty < \gamma, \tag{64}$$

where $F_l\left(P_{aug}, C\right)$ is the lower linear fractional transformation (LFT) between $P_{aug}(s)$ and $C(s)$ and is defined by

$$\begin{pmatrix} o_1 \\ o_2 \end{pmatrix} = F_l\left(P_{aug}, C\right) \begin{pmatrix} x_d \\ \Omega_w \end{pmatrix} \tag{65}$$

From Figure 13-b, we have

$$\begin{cases} o_1 = W_1 S x_d - W_1 S W_3 \Omega_w \\ o_2 = W_2 C S x_d - W_2 C S W_3 \Omega_w, \end{cases} \tag{66}$$

where $S = \frac{1}{(1+CG)}$ is the sensitivity function. With (65) and (66), we have

$$F_l\left(P_{aug}, C\right) = \begin{pmatrix} W_1 S & -W_1 S W_3 \\ W_2 C S & -W_2 C S W_3 \end{pmatrix}. \tag{67}$$

Using (64) and (67), the H_∞ problem becomes in finding an optimal value $\gamma > 0$ and $C(s)$ such that

$$\begin{array}{ll} \|W_1 S\|_\infty < \gamma; & \|-W_1 S W_3\|_{<\infty} < \gamma; \\ \|W_2 C S\|_\infty < \gamma; & \|-W_2 C S W_3\|_\infty < \gamma \end{array} \tag{68}$$

which are also respected if we have

$$\begin{array}{ll} |S| < \frac{\gamma}{|W_1|}; & |S| < \frac{\gamma}{|W_1 W_3|}; \\ |CS| < \frac{\gamma}{|W_2|}; & |CS| < \frac{\gamma}{|W_2 W_3|}; \end{array} \tag{69}$$

where $\frac{1}{W_1}$, $\frac{1}{W_1 W_3}$, $\frac{1}{W_2}$, and $\frac{1}{W_2 W_3}$ are called gabarits.

4) Derivation of the weighting functions: The weighting functions calculated from the gabarits are chosen according to the specifications defined in Section. V-E2. For the tracking performance specifications, we choose

$$\frac{1}{W_1} = \frac{s+1}{s+1000} \quad \Rightarrow \quad W_1 = \frac{s+1000}{s+1}. \tag{70}$$

For the command moderation, we choose

$$\frac{1}{W_1 W_2} = \frac{v^{\max}}{x_d^{\max}} = \frac{40\mu m}{40\mu m} = 1 \tag{71}$$

from which we deduce the weighting W_2

$$W_2 = \frac{s+1}{s+1000}. \tag{72}$$

For the disturbance rejection, we have

$$\frac{1}{W_1 W_3} = \frac{e^{\max}}{\Omega_w^{\max}} = \frac{0.1\mu m}{3.825\mu m} = 0.026. \tag{73}$$

Then we deduce the weighting W_3 as

$$W_3 = 0.026 \frac{s+1}{s+1000}. \tag{74}$$

5) Controller calculation: The controller $C(s)$ has been calculated by applying the Doyle-Glover algorithm [46], [47] to the problem (69). We find a controller of order equal to 11. In order to have a simpler controller, we have reduced its size up to 5 without affecting the performance of the closed-loop system. The reduction method was based on the balanced realization/reduction technique [48]. The reduced controller and the optimal value of γ are

$$\begin{cases} C(s) = \frac{0.016\left(s+7.9\times10^6\right)\left(s^2+971s+4.6\times10^5\right)\left(s^2+43s+1.4\times10^7\right)}{\left(s+8.8\times10^4\right)(s+974)(s+1)\left(s^2+1153s+1.6\times10^7\right)} \\ \gamma = 1.69. \end{cases} \tag{75}$$

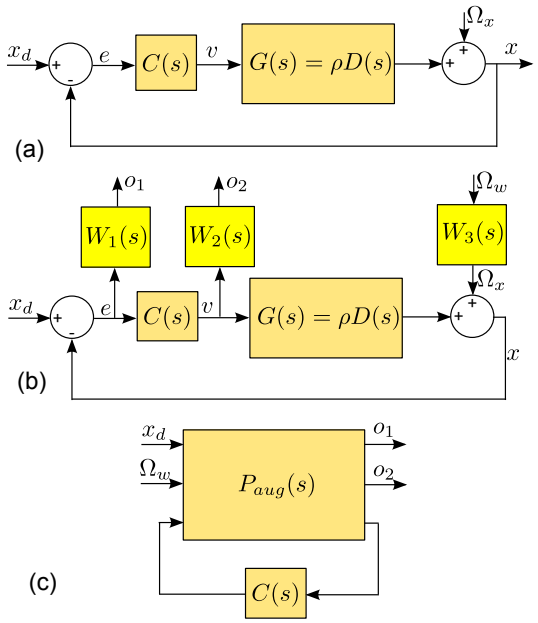

Fig. 13. Diagram used for the feedback controller $C(s)$ synthesis. (a) block diagram of the closed-loop system, (b) block diagram of the closed loop augmented with the weighting functions $W_1(s)$, $W_2(s)$ and $W_3(s)$, (c) standard scheme of the weighted closed-loop.

6) Experimental results: The calculated feedback controller $C(s)$ has been implemented to control the PEA with the inverse compensator $\hat{\mathcal{P}}^{-1}$. The first experiment consists in applying a series of step reference x_d to the closed-loop in order to verify that there is no instability after a long period of time. Figure 14-a pictures the results which effectively show that the stability of the closed-loop system is maintained when the constant input voltage is maintained over more than 1.5s. Figure 14-b pictures a zoom of the step response displacement. It shows that the settling time is less than 2ms, the overshoot is null and and the steady state error is negligible. We therefore conclude that the tracking performances are satisfied.

The next experiment shown in Figure 15 (a), (b), (c), and (d) considers a sinusoidal input reference x_d with amplitude of 40μm at 0.01Hz, 0.1Hz, 1Hz, and 10Hz. Figure 15-e pictures the tracking error $x_d(t) - x(t)$ at 0.01Hz with the absolute tracking error of 0.02μm and the root-mean-square (RMS) of 260nm. Tab. I summarizes the absolute error and the RMS of the tracking error at different excitation frequencies. We can observe from this table and Figure 15-d that there is a slight phase-lag (about 20^o) at $f = 10$Hz which yields higher RMS error. In fact, the phase-lag starts to exist slightly before the bandwidth of the closed-loop system, and in this case, the bandwidth is of 67Hz (see next experiment). In some applications where the references are known in advance or are repetitive, the lag is not necessarily drastic since it only shifts in the time domain the execution of the tasks without affecting the tracking. In such a case, the 3dB bandwidth is more important. In order to analyze the bandwidth of the closed-loop, we characterized the harmonic response of the

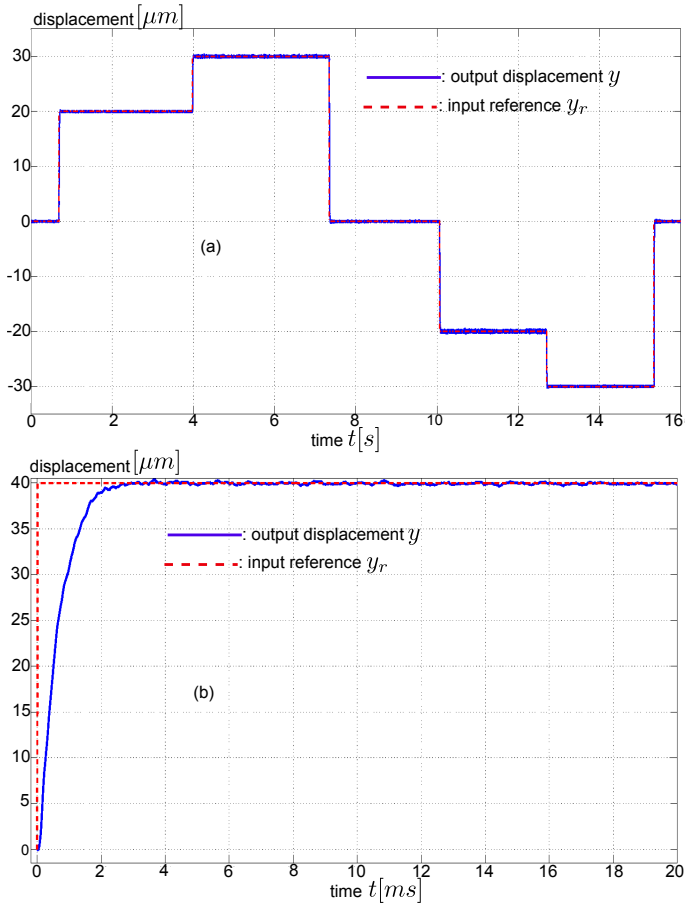

Fig. 14. Feedforward-feedback control of the PEA. (a): responses to a series of steps. (b): a step response.

closed-loop. This is presented in the next paragraph.

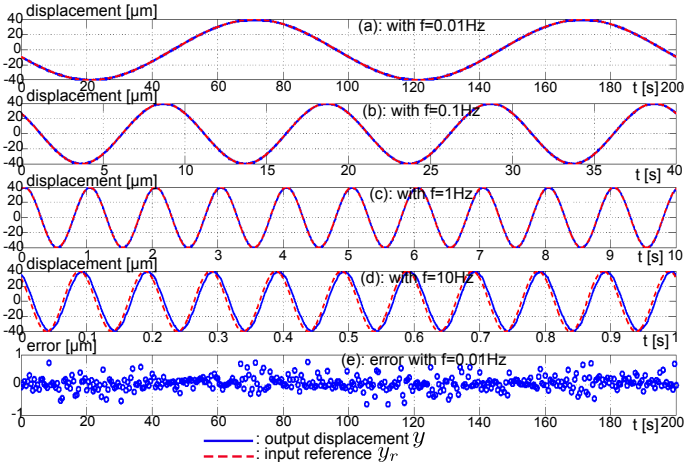

Fig. 15. Comparison between the reference input and the output displacement at excitation frequencies of (a) 0.01Hz, (b) 0.1Hz, (c) 1Hz, and (d) 10Hz., (e) the tracking error at 0.01Hz.

The last experiment consists of applying another sinusoidal input reference but with frequency ranging between 0.01Hz and 1kHz such that the harmonic output displacement of the

TABLE I
TRACKING ERROR $x_d(t) - x(t)$

frequency [Hz]	0.01	0.1	1	10
absolute error [μm]	0.025	0.106	0.07	0.275
RMS [μm]	0.236	0.238	0.814	7.353

closed-loop (hysteresis compensator + feedback controller) can be characterized. Figure 16 pictures the corresponding magnitude and phase. In the figure, the harmonic response of the PEA without the feedforward-feedback control is also plotted, that is without the hysteresis compensator $\hat{\mathcal{P}}$ and the feedback controller $C(s)$. We observe resonance at about 500Hz that is completely removed when controlled by the closed-loop controller. We also notice the hysteresis that is observed as the decay of the magnitude at low excitation frequencies is compensated as it is flatten with the control. Finally, we can calculate from Figure 16-a the 3dB bandwidth of the closed-loop: 67dB. This bandwidth can still be increased by modifying the specifications given in Section V used to calculate the H_∞ controller. Figure 16-b shows that the phase of the controlled system starts to lag slightly before 10Hz. This has been observed in Figure 15-d. Also, it is possible to introduce a constraint on this phase-lag in the specifications used for the calculation of the H_∞ controller if required.

The experiments demonstrated the efficiency of the controller despite of the RHP zeros see (60). The calculation of the feedback controller was carried out with a formula that describes the output of the inverse compensation. We have therefore demonstrated in this experimental case an example of utilization of this formula.

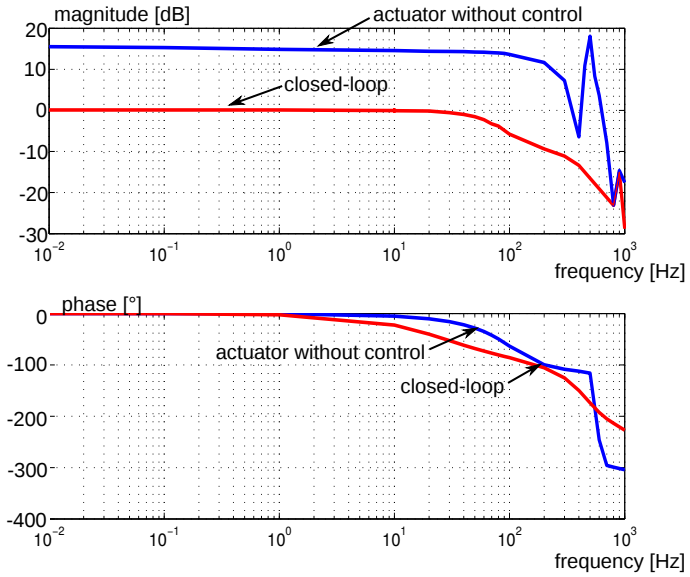

Fig. 16. Magnitude and phase of the closed-loop compared with the magnitude and phase of the PEA without control.

VI. CONCLUSIONS

A formula that describes the output of the inverse compensation is obtained in a compact way when the inverse Prandtl-Ishlinskii model is applied to compensate for the hysteresis nonlinearity. The output of the inverse compensation is characterized by a linear reversible term and a bounded nonlinear term. This formula can be used in closed-loop control systems with controlled plants to reduce the tracking errors. An experimental case with a piezoelectric actuator (PEA) has also been carried out where the formula is used to synthesize an H_∞ controller that commands this. The experimental results demonstrate the efficiency of the control scheme and therefore the benefit of using the formula to synthesize the latter.

ACKNOWLEDGMENT

This work is supported by the French ANR-JCJC C-MUMS-project (National young investigator project ANR-12-JS03007.01: Control of Multivariable Piezoelectric Microsystems with Minimization of Sensors).

REFERENCES

[1] M. Rakotondrabe, C. Clevy, and P. Lutz, "Complete open loop control of hysteretic, creeped, and oscillating piezoelectric cantilevers," *IEEE Transactions on Automation Science and Engineering*, vol. 7, no. 3, pp. 440-450, 2010.

[2] Q. Xu, "New Flexure Parallel-Kinematic Micropositioning System with Large Workspace," *IEEE Transactions on Robotics*, vol. 28, no. 2, pp. 478-491, 2012.

[3] Y. Qin, Y. Tian, D. Zhang, B. Shirinzadeh, and S. Fatikow, "A novel direct inverse modeling approach for hysteresis compensation of piezoelectric actuator in feedforward applications," *IEEE/ASME Transactions on Mechatronics*, vol. 18, no. 3, pp. 981-989, 2013.

[4] J. Rodriguez-Fortun, J. Orus, J. Alfonso, F. Gimeno, and J. Castellanos, "Flatness-based active vibration control for piezoelectric actuators," *IEEE/ASME Transactions on Mechatronics*, vol. 18, no. 1, pp. 221-229, 2013.

[5] K. Leang, Q. Zou, and S. Devasia, "Feedforward control of piezoactuators in atomic force microscope systems: inversion-based compensation for dynamics and hysteresis," *IEEE Control Systems Magazine*, vol. 19, no. 1, pp. 70-82, 2009.

[6] M. Grossard, M. Boukallel, N. Chaillet, and C. Rotinat-Libersa, "Modeling and robust control strategy for a control-optimized piezoelectric microgripper," *IEEE/ASME Transactions on Mechatronics*, vol. 16, no. 4, pp. 674-683, 2011.

[7] Y. Zhang, M. Han, M. Yu, C. Shee, and W. Ang, "Automatic hysteresis modeling of piezoelectric micromanipulator in vision-guided micromanipulation systems," *IEEE/ASME Transactions on Mechatronics*, vol. 17, no.3, pp. 547-553, 2012.

[8] R. C. Smith, *Smart Material Systems*, Philadelphia, PA, Springer-Verlag, 2005.

[9] C. Visone, "Hysteresis modelling and compensation for smart sensors and actuators," *Journal of Physics: Conference Series*, vol. 138, DOI:10.1088/1742-6596/138/1/012028, 2008.

[10] X. Tan and J. Baras, "Modeling and control of hysteresis in magnetostrictive actuators," *Automatica*, vol. 40, no. 9, pp. 1469-1480, 2004.

[11] R. Iyer, X. Tan, and P. S. Krishnaprasad, "Approximate inversion of the Preisach hysteresis operator with applications to control of smart actuators," *IEEE Transactions on Control Systems Technology*, vol. 50, no. 6, pp. 798-810, 2005.

[12] M. Al Janaideh and P. Krejčí, "Inverse rate-dependent Prandtl-Ishlinskii model for feedforward compensation of hysteresis in a piezomicropositioning actuator," *IEEE/ASME Transactions on Mechatronics*, vol 18, no. 5, pp.1498-1507, 2013.

[13] M. Al Janaideh, "About the output of the inverse compensation of the Prandtl-Ishlinskii model," *Proceedings of the American Control Conference,* pp. 247-252, Washington, DC, 2013.

[14] M. Al Janaideh and P. Krejci, "An inversion formula for a PrandtlIshlinskii operator with time dependent thresholds," *Physica B*, vol. 406, no. 8, pp. 1528-1532, 2011.

[15] P. Krejci, M. Al Janaideh, and F. Deasy, "Inversion of hysteresis and creep operators ," *Physica B*, vol. 407, no. 8, pp. 1354-1356, 2012.

[16] M. Rakotondrabe, "Classical Prandtl-Ishlinskii modeling and inverse multiplicative structure to compensate hysteresis in piezoactuators", *Proceedings of the American Control Conference*, pp.1646-1651, Montral Canada, June 2012.

[17] G. Aguirre, T. Janssens, H. Van Brussel, and F. Al-Bender, "Asymmetric hysteresis compensation in piezoelectric actuators," *Mechanical Systems and Signal Processing*, 2012, vol. 30, pp. 218-231.

[18] F. Al-Bender, W. Symens, J. Swevers, and H. Van Brussel, "Theoretical analysis of the dynamic behavior of hysteresis elements in mechanical systems," *International Journal of Non-Linear Mechanics*, vol. 39, no. 10, 2004, pp. 1721-1735.

[19] M. Rakotondrabe, "Bouc-Wen modeling and inverse multiplicative structure to compensate hysteresis nonlinearity in piezoelectric actuators," *IEEE Transactions on Automation Science and Engineering*, vol. 8, no. 2, pp. 428-431, 2011.

[20] T. S. Low and W. Guo, "Modeling of a three-layer piezoelectric bimorph beam with hysteresis," *Journal Microelectromechanical Systems*, vol .4, no. 4, pp. 230-237, 1995.

[21] S. Dutta and F. Ghorbel, "Differential hysteresis modeling of a shape memory alloy wire actuator," *IEEE/ASME Transactions on Mechatronics,* vol. 10, no. 2, pp. 189-197, 2005.

[22] M. Al Janaideh, R. Naldi, L. Marconi, and P. Krejčí, "A hybrid system for a class of hysteresis nonlinearity: modeling and compensation", *Proceedings of the IEEE Conference on Decision and Control*, Maui, HI, pp. 5380-5385, 2012.

[23] M. Al Janaideh and D. S. Bernstein, "Inversion-Free Adaptive Control of Uncertain Systems with SMA Actuation," *Proceedings of the American Control Conference,* pp. 3585-3590, Washington, DC, 2013.

[24] R. Gorbet, K. Morris, and D. Wang, "Passivity-based stability and control of hysteresis in smart actuators," *IEEE Transactions on Control Systems Technology*, vol. 9, no. 1, pp. 5-16, 2001.

[25] M. Rakotondrabe, Y. Haddab and P. Lutz, "Plurilinear modeling and discrete -synthesis control of a hysteretic and creeped unimorph piezoelectric cantilever", *IEEE - ICARCV, International Conference on Automation, Robotics, Control and Vision*, pp. 57-64, Grand Hyatt Singapour, December 2006.

[26] M. Rakotondrabe, Y. Haddab and P. Lutz, "Quadrilateral modelling and robust control of a nonlinear piezoelectric cantilever", *IEEE Transactions on Control Systems Technology (T-CST)*, vol. 17, no. 3, pp. 528-539, 2009.

[27] B. Jayawardhana, H. Logemann, and E. Ryan, "PID control of second-order systems with hysteresis," *International Journal of Control*, vol. 8, no. 8, pp. 13-31, 2008.

[28] L. Riccardi, D. Naso, B. Turchiano, H. Janocha and D. K. Palagachev, "On PID control of dynamic systems with hysteresis using a Prandtl-Ishlinskii model," *Proceedings of the American Control Conference,* pp. 1670-1675, 2012.

[29] L. Riccardi, D. Naso, B. Turchiano, and H. Janocha, "Design of linear feedback controllers for dynamic systems with hysteresis," *IEEE Transactions on Control Systems Technology,* vol. 22, no. 4, pp. 1268-1280, 2014.

[30] M. Al Janaideh, "Generalized Prandtl-Ishlinskii hysteresis model and its analytical inverse for compensation of hysteresis in smart actuators," PhD thesis, Concordia University, Montral, Canada, 2009.

[31] X. Fan and R. Smith, "Model-based $\mathcal{L}1$ adaptive control of hysteresis in smart materials," *Proceedings of the IEEE Conference on Decision and Control*, Cancun, Mexico, pp. 3251-3256, 2008.

[32] M. Rakotondrabe, K. Rabenorosoa, J. Agnus and N. Chaillet, "Robust feedforward-feedback control of a nonlinear and oscillating 2-dof piezocantilever", *IEEE Transactions on Automation Science and Engineering (T-ASE)*, vol. 8, no. 3, pp. 506-519, 2011.

[33] M. Brokate and J. Sprekels, *Hysteresis and Phase Transitions*, New York, NY, Springer, 1996.

[34] P. Krejci, *Hysteresis, convexity and dissipation in hyperbolic equation*, Gakuto, International series of Math Science and applications, 1986.

[35] A. Esbrook, X. Tan, and H. K. Khalil, "Control of Systems With Hysteresis via Servocompensation and Its Application to Nanopositioning," *IEEE Transactions on Control Systems Technology*, vol. 21, no. 3, pp. 725-738, 2013.

[36] M. Edardar, X. Tan, and H. K. Khalil, "Design and Analysis of Sliding Mode Controller Under Approximate Hysteresis Compensation," *IEEE Transactions on Control Systems Technology*, DOI:10.1109/TCST.2014.2329187, June 20, 2014.

[37] M. Edardar, "Robust control of systems with piecewise linear hysteresis," PhD Dissertation, Michigan State University, 2013.

[38] M. Edardar, X. Tan, and H. Khalil, "Sliding-Mode Tracking Control of Piezo-Actuated Nanopositioners," *Proceedings of the American Control Conference, pp. 3825-3830, Montral Canada*, June 2012.

[39] J. Agnus, N. Chaillet, C. Clévy, S. Dembélé, M. Gauthier, Y. Haddab, G. Laurent, P. Lutz, N. Piat, K. Rabenorosoa, M. Rakotondrabe, and B. Tamadazte, "Robotic microassembly and micromanipulation at FEMTO-ST," *Journal of Micro-Bio Robotics*, vol. 8, no. 2, pp. 91-106, 2013.

[40] R. Wood, J. Whitney, and B. Finio, "Mechanics and Actuation for Flapping- Wing Robotic Insects," Published Editors: R. Blockley and W. Collection, *Encyclopedia of Aerospace Engineering*, pp. 4393-4406, 2011.

[41] G. Bining, C. F. Quate, and Ch. Berger, "Atomic Force Microscope," *APS Physical Review Letters*, vol. 56, no. 9, pp. 930-933, 1986.

[42] Y. Zhu, W. Liu, K. Jia, W. Liao, and H. Xie, "A piezoelectric unimorph actuator based tip-tilt-piston micromirror with high fill factor and small tilt and lateral shift", *Sensors and Actuators A: Physical*, vol. 167, no. 2, pp. 495-501, 2011.

[43] S. Lescano, D. Zlatanov, M. Rakotondrabe and N. Andreff, "Kinematic Analysis of a Meso Scale Parallel Robot for Laser Phonomicrosurgery," Springer IAK, *(International Conference on Interdisciplinary Applications in Kinematic)*, Lima Peru, September 2013.

[44] L. Ljung, *System identification toolbox*, The Matlab user's guide, 1988.

[45] G. J. Balas, J. C. Doyle, K. Glover, A. Packard and R. Smith, μ*-analysis and synthesis toolbox*, The Mathworks User's Guide-3, 2001.

[46] K. Glover and J. C. Doyle, "State-space formulae for all stabilizing controllers that satisfy an H_∞-norm bound and relations to risk sensivity," *Systems & Control Letters*, vol. 11, no. 3, pp.167-172, 1988.

[47] J. C. Doyle, K. Glover, P. K. Khargonekar and B. A. Francis, "State-space solutions to standard H_2 and H_∞ control problems," *IEEE Transactions on Automatic Control*, AC-34, no. 8, pp. 831-846, 1989.

[48] B. C. Moore, "Principal component analysis in linear systems: controllability, observability and model reduction," *IEEE Transaction on Automatic Control,* AC-26, no. 1, pp. 17-32, 1981.